THE ASTROPHYSICAL JOURNAL, 483:121–135, 1997 July 1

THE STABILITY OF RADIATIVELY COOLING JETS. I. LINEAR ANALYSIS

PHILIP E. HARDEE
Department of Physics and Astronomy, University of Alabama, 206 Gallalee Hall, Box 870324, Tuscaloosa, AL 35487-0324;
hardee@venus.astr.ua.edu

AND

JAMES M. STONE
Department of Astronomy, University of Maryland, College Park, MD 20742; jstone@ophir.astro.umd.edu

Received 1996 June 11; accepted 1997 January 30

ABSTRACT

The results of a spatial stability analysis of a two-dimensional slab jet, in which optically thin radiative cooling is dynamically important, are presented. We study both magnetized and unmagnetized jets at external Mach numbers of 5 and 20. We model the cooling rate by using two different cooling curves: one appropriate to interstellar gas, and the other to photoionized gas of reduced metallicity. Thus, our results will be applicable to both protostellar (Herbig-Haro) jets and optical jets from active galactic nuclei.

We present analytical solutions to the dispersion relations in useful limits and solve the dispersion relations numerically over a broad range of perturbation frequencies. We find that the growth rates and wavelengths of the unstable Kelvin-Helmholtz (K-H) modes are significantly different from the adiabatic limit, and that the form of the cooling function strongly affects the results. In particular, if the cooling curve is a steep function of temperature in the neighborhood of the equilibrium state, then the growth of K-H modes is reduced relative to the adiabatic jet. On the other hand, if the cooling curve is a shallow function of temperature, then the growth of K-H modes can be enhanced relative to the adiabatic jet by the increase in cooling relative to heating in overdense regions. Inclusion of a dynamically important magnetic field does not strongly modify the important differences between an adiabatic jet and a cooling jet, provided the jet is highly supermagnetosonic and not magnetic pressure–dominated. In the latter case, the unstable modes behave more like the transmagnetosonic magnetic pressure–dominated adiabatic limit. We also plot fluid displacement surfaces associated with the various waves in a cooling jet in order to predict the structures that might arise in the nonlinear regime. This analysis predicts that low-frequency surface waves and the lowest order body modes will be the most effective at producing observable features in the jet.

Subject headings: galaxies: jets — hydrodynamics — instabilities — ISM: jets and outflows — MHD

1. INTRODUCTION

The structure and morphology of astrophysical jets can be affected by a variety of dynamical processes, for example, interaction with ambient material or variability in the parameters of the jet itself. In addition, it has long been recognized that even steady isolated jets may form structure through the growth of Kelvin-Helmholtz (K-H) modes. For this reason, the stability properties of supermagnetosonic astrophysical jets have been the subject of intense study. To date, almost all such studies have been confined to adiabatic jets (e.g., see the review by Birkinshaw 1991) with application to extragalactic radio sources. Such studies find that adiabatic supermagnetosonic jets are always unstable. Moreover, it has been shown for a limited number of specific sources (e.g., 3C 449; Hardee, Cooper, & Clarke 1994) that the apparent sinusoidal pattern in the plane of the sky can be explained successfully by the unstable growth of helical twisting excited by a small precessional or orbital motion of the central engine.

Some of the finest examples of astrophysical jets, however, are nonadiabatic flows in which the cooling time due to optically thin radiation is comparable to or less than the dynamical time. Examples of nonadiabatic or "cooling" jets include the protostellar or Herbig-Haro jets associated with star-forming regions (Edwards, Ray, & Mundt 1993; Ray 1996) and jets in Seyfert galaxies. In this case, the loss of thermal energy from the system can have significant effects on the dynamics of the jet, e.g., Falle, Innes, & Wilson (1987) and Blondin, Fryxell, & Königl (1990), making the results of studies of adiabatic jets largely inapplicable to these systems. In a series of papers, Stone & Norman (1993a, 1993b, 1994) extended earlier work by combining a more realistic cooling model with three-dimensional simulations. These studies reveal that cooling jets sweep up dense shells of shocked jet and ambient gas that are strongly fragmented into knots and clumps. These results are consistent with those of a number of other workers (Gouviea dal Pino & Benz 1993; Chernin et al. 1994) who use different numerical techniques.

Thus, while a number of studies have revealed much about the *propagation* of cooling jets, the *stability* properties of such flows, and the nonlinear dynamics and structure of K-H unstable cooling jets, is less well understood. Bührke, Mundt, & Ray (1988, hereafter BMR) were the first to propose that the emission knots observed in some protostellar jets could be produced by the growth of the K-H pinch modes. Subsequently, kinematic studies have discovered that in many cases, internal knots can be attributed to variability in the outflow instead (Reipurth 1989). Hydrodynamical simulations of pulsed jets reveal the growth of knots similar to those observed in protostellar jets (Stone & Norman 1993b; Gouviea dal Pino & Benz 1994). Still, the asymmetric pattern of knots observed in some systems (e.g., HH 47; Heathcote et al. 1996) is difficult to account for by pulsing alone, and this suggests that at some level, K-H instability may play a role in determining jet structure. However, as

BMR recognized, applying the results of stability analyses performed for adiabatic jets to cooling jets can be misleading, since cooling can alter the growth rates and wavelengths of K-H modes. Thus, interpreting the structure of cooling jets quantitatively as being the result of K-H modes requires a self-consistent stability analysis, including the effects of radiative cooling.

To date, the only stability analyses of cooling jets that have been presented in the literature have been limited in scope. For example, Massaglia et al. (1992) have considered the effect of cooling on the symmetric K-H pinching mode of a cylindrical fluid jet. They performed a temporal analysis and only solved the dispersion relation at two discrete wavenumbers.

In this paper, we report the results of a comprehensive linear stability analysis of a two-dimensional slab jet with radiative cooling. Here we perform a spatial stability analysis. We give analytic solutions to the dispersion relation in several useful limits and use numerical techniques to find the solutions as a function of frequency. We study the effect of different cooling curves (one appropriate to photoionized gas and jets in active galaxies, and one appropriate to interstellar gas and protostellar jets). We also study stability properties in the presence of magnetic fields. In this paper, we find that there are substantial differences in the growth rates and wavelengths of unstable K-H modes between cooling and adiabatic jets. In a companion paper (Stone, Xu, & Hardee 1997, hereafter Paper II), we present time-dependent hydrodynamical simulations that follow the growth of K-H modes into the nonlinear regime.

We choose to study a slab jet in this paper for a number of reasons. A slab jet is spatially resolved along two Cartesian axes and is effectively infinite in extent in the third dimension. Analysis of the stability properties of slab jets has revealed that the symmetric pinching mode and asymmetric sinusoidal mode are qualitatively similar to the pinch and helical modes of a cylindrical jet (Hardee & Norman 1988). Thus, the asymmetric sinusoidal mode of a slab jet becomes a direct analog to the helical mode of a three-dimensional jet. We note that on the adiabatic jet, the asymmetric sinusoidal mode of a slab jet and the helical mode of a cylindrical jet are predicted to grow more rapidly than the accompanying symmetric pinch mode. The numerical computation of the nonlinear evolution of a two-dimensional slab jet is simplified greatly by the reduction in computer memory and CPU requirements in comparison with a fully three-dimensional jet, making parameter space surveys possible. We will report on the stability properties and nonlinear evolution of a fully three-dimensional cooling jet in a future paper.

The organization of this paper is as follows. In § 2, we derive the linearized dispersion relations for a cooling slab jet and discuss the forms of the different cooling functions adopted here. In § 3, we present solutions to the dispersion relations in several useful limits. In § 4, we present numerical solutions to the dispersion relations. In § 5, we compare and contrast our results with studies of adiabatic jets, and in § 6 we summarize our results.

2. LINEARIZED STABILITY ANALYSIS

Let us model a jet as a slab bounded by $|x| = R$, having a uniform density ρ_{jt} and a uniform internal magnetic field $\boldsymbol{B}_{jt}$ at an angle ϕ_{jt} with respect to a uniform velocity $\boldsymbol{u} = u_z$. The external medium has a uniform density ρ_{ex} and contains a uniform magnetic field $\boldsymbol{B}_{ex}$ at an angle ϕ_{ex} with respect to the jet velocity. The jet is in static total pressure balance with the external medium, i.e., $p^*_{ex} \equiv p_{ex} + B^2_{ex}/8\pi = p^*_{jt} \equiv p_{jt} + B^2_{jt}/8\pi$. The initial equilibrium state must satisfy

$$\frac{\partial \rho_0}{\partial t} + \nabla \cdot (\rho_0 \boldsymbol{u}_0) = 0 ,$$

$$\rho_0 \frac{\partial \boldsymbol{u}_0}{\partial t} = -\nabla p_0 + \frac{[(\nabla \times \boldsymbol{B}_0) \times \boldsymbol{B}_0]}{4\pi} ,$$

$$\frac{D}{Dt} p_0 - \Gamma \frac{p_0}{\rho_0} \frac{D}{Dt} \rho_0 = (\Gamma - 1)(H_0 - C_0) ,$$

where $H(p, \rho)$ and $C(p, \rho)$ are the heating and cooling rates per unit volume, respectively, Γ is the adiabatic index, $D/Dt \equiv \partial/\partial t + \boldsymbol{u} \cdot \partial/\partial \boldsymbol{x}$, and the subscript 0 implies an initial equilibrium value. An initial equilibrium state implies that $H_0 \equiv H(p_0, \rho_0) = C_0 \equiv C(p_0, \rho_0)$.

The general approach to analyzing the stability properties of this system is to linearize the one-fluid MHD equations of continuity, momentum, and energy within each medium in which the flow velocity $\boldsymbol{u} = 0$. The flow velocity is then reintroduced when solutions are matched at the jet boundary. The linearized MHD equations that are relevant to our model become (e.g., Hunter & Whitaker 1989)

$$\frac{\partial \rho_1}{\partial t} + \nabla \cdot (\rho_0 \boldsymbol{u}_1) = 0 ,$$

$$\rho_0 \frac{\partial \boldsymbol{u}_1}{\partial t} = -\nabla p_1 + \frac{[(\nabla \times \boldsymbol{B}_0) \times \boldsymbol{B}_1 + (\nabla \times \boldsymbol{B}_1) \times \boldsymbol{B}_0]}{4\pi} ,$$

$$\frac{D}{Dt} p_1 - \Gamma \frac{p_0}{\rho_0} \frac{D}{Dt} \rho_1 = (\Gamma - 1)(H_1 - C_1) ,$$

where the density, velocity, pressure, magnetic field, and heating and cooling rates are written as $\rho = \rho_0 + \rho_1$, $\boldsymbol{u} = \boldsymbol{u}_1$, $p = p_0 + p_1$, $\boldsymbol{B} = \boldsymbol{B}_0 + \boldsymbol{B}_1$, $H = H_0 + H_1$, $C = C_0 + C_1$, and subscript 1 refers to a perturbation to the equilibrium quantity.

The perturbed part of the heating and cooling rates in the energy equation can be written as

$$H_1 - C_1 = \left(\frac{\partial H}{\partial p}\bigg|_\rho - \frac{\partial C}{\partial p}\bigg|_\rho\right)p_1 + \left(\frac{\partial H}{\partial \rho}\bigg|_p - \frac{\partial C}{\partial \rho}\bigg|_p\right)\rho_1 ,$$

and following Hunter & Whitaker, we rewrite the energy equation in the form

$$\frac{D}{Dt}\,p_1 + F_p p_1 = \Gamma\,\frac{p_0}{\rho_0}\left(\frac{D}{Dt}\,\rho_1 + F_\rho \rho_1\right),$$

where

$$F_p \equiv (\Gamma - 1)\left(\frac{\partial C}{\partial p}\bigg|_\rho - \frac{\partial H}{\partial p}\bigg|_\rho\right),$$

and

$$F_\rho \equiv \frac{\Gamma - 1}{a^2}\left(\frac{\partial H}{\partial \rho}\bigg|_p - \frac{\partial C}{\partial \rho}\bigg|_p\right),$$

where the sound speed $a^2 \equiv \Gamma p_0/\rho_0$. It is often more useful to write the heating and cooling rates per unit volume as $H(T, \rho)$ and $C(T, \rho)$. With this choice, it can be shown that

$$F_p = \frac{\Gamma(\Gamma - 1)}{\rho_0 a^2}\,\boldsymbol{C}\left(\frac{\partial \ln C}{\partial \ln T}\bigg|_\rho - \frac{\partial \ln H}{\partial \ln T}\bigg|_\rho\right),$$

and

$$F_\rho = \frac{\Gamma - 1}{\rho_0 a^2}\,\boldsymbol{C}\left(\frac{\partial \ln C}{\partial \ln T}\bigg|_\rho - \frac{\partial \ln C}{\partial \ln \rho}\bigg|_T + \frac{\partial \ln H}{\partial \ln \rho}\bigg|_T - \frac{\partial \ln H}{\partial \ln T}\bigg|_\rho\right),$$

where $\boldsymbol{C} \equiv C_0 = H_0$.

In slab geometry, we look for perturbations ρ_1, u_1, p_1, and $\boldsymbol{B}_1$ of the form

$$f_1(x, y, z) = f_1(x)\,\exp\,[i(k_y y + k_z z - \omega t)]\,, \tag{1}$$

where y is perpendicular to the flow in the plane of the slab jet. Note that spatial growth of a perturbation corresponds to a negative imaginary part of the wavenumber and that temporal growth of a perturbation corresponds to a positive imaginary part of the wave frequency. With this form for the perturbations, a differential equation for the dependence of the total pressure perturbation $p_1^* \equiv p_1 + \boldsymbol{B}_1 \cdot \boldsymbol{B}_0/4\pi$ within each medium as a function of x can be written in the form

$$\frac{\partial^2 p_1^*}{\partial x^2} + \beta^2 p_1^* = 0\,, \tag{2}$$

where, in general,

$$\beta \equiv \left[-k^2 + \frac{(\omega')^4}{(\omega')^2(a^2/Q + V_A^2) - k^2\cos^2(\theta - \phi)V_A^2 a^2/Q}\right]^{1/2}. \tag{3}$$

In equation (3), $V_A = (B_0^2/4\pi\rho_0)^{1/2}$ is the Alfvén speed, $k^2 = k_y^2 + k_z^2$, $k_z = k\cos\theta$, $\omega' \equiv (\omega - ku\cos\theta)$ is the Doppler-shifted frequency, and u is the flow velocity of the fluid with respect to the rest (observer) frame. Note that $V_A\cos(\theta - \phi)$ is the projection of the Alfvén velocity along the wavevector $\boldsymbol{k}$. The heating and cooling rates are contained in the dimensionless quantity

$$Q \equiv \frac{1 + iF_p/\omega'}{1 + iF_\rho/\omega'}\,.$$

Note that the adiabatic case is recovered by setting $Q = 1$. The solutions are understood most easily when written in the form

$$p_{1\,\mathrm{jt}}^*(x) = C_{\mathrm{as}}\sin(\beta_{\mathrm{jt}}x) + C_s\cos(\beta_{\mathrm{jt}}x) \tag{4}$$

inside the jet, and

$$p_{1\,\mathrm{ex}}^*(x) = C_\pm\, e^{\pm i\beta_{\mathrm{ex}}x} \tag{5}$$

outside the jet, where the plus or minus sign is chosen so that $p_{1\,\mathrm{ex}}^*(x) \to 0$ as $|x| \to \infty$. In equation (4),

$$\beta_{\mathrm{jt}} = \left[-k^2 + \frac{(\omega - k\cos\theta u)^4}{(\omega - k\cos\theta u)^2(a_{\mathrm{jt}}^2/Q_{\mathrm{jt}} + V_{\mathrm{A,jt}}^2) - k^2\cos^2(\theta - \phi_{\mathrm{jt}})V_{\mathrm{A,jt}}^2 a_{\mathrm{jt}}^2/Q_{\mathrm{jt}}}\right]^{1/2}, \qquad Q_{\mathrm{jt}} = \frac{1 + iF_p^{\mathrm{jt}}/(\omega - k\cos\theta u)}{1 + iF_\rho^{\mathrm{jt}}/(\omega - k\cos\theta u)},$$

and in equation (5),

$$\beta_{\rm ex} = \left[-k^2 + \frac{\omega^4}{\omega^2(a_{\rm ex}^2/Q_{\rm ex} + V_{\rm A,ex}^2) - k^2 \cos^2(\theta - \phi_{\rm ex}) V_{\rm A,ex}^2 a_{\rm ex}^2/Q_{\rm ex}} \right]^{1/2}, \qquad Q_{\rm ex} = \frac{1 + iF_p^{\rm ex}/\omega}{1 + iF_\rho^{\rm ex}/\omega}.$$

In the expressions above, we have chosen the rest frame to be the reference frame of the external medium.

At $|x| = R$, we require that the total pressure be continuous across the boundary, i.e., $p_{1\rm jt}^*(R) = p_{1\rm ex}^*(R)$, and that the fluid displacement inside and outside the jet in the x-direction must be equal at the jet boundary, i.e., $\xi_x^{\rm jt}(R) = \xi_x^{\rm ex}(R)$, where the fluid displacement in the x-direction is given by

$$\xi_x^{\rm jt} = \frac{1}{\chi_{\rm jt}} \frac{\partial p_{1\rm jt}^*}{\partial x} \quad \text{and} \quad \xi_x^{\rm ex} = \frac{1}{\chi_{\rm ex}} \frac{\partial p_{1\rm ex}^*}{\partial x}. \tag{6}$$

In equations (6),

$$\chi_{\rm jt} = \rho_{\rm jt}[(\omega - k\cos\theta u)^2 - k^2 \cos^2(\theta - \phi_{\rm jt}) V_{\rm A,jt}^2],$$

and

$$\chi_{\rm ex} = \rho_{\rm ex}[\omega^2 - k^2 \cos^2(\theta - \phi_{\rm ex}) V_{\rm A,ex}^2].$$

The requirement that the two jet boundaries be coupled, along with equations (4), (5), and (6), and the boundary conditions on the pressure and the displacement, can be shown to result in two dispersion relations:

$$\frac{\beta_{\rm jt}}{\chi_{\rm jt}} \tan(\beta_{\rm jt} R) = -i \frac{\beta_{\rm ex}}{\chi_{\rm ex}}, \tag{7}$$

and

$$\frac{\beta_{\rm jt}}{\chi_{\rm jt}} \cot(\beta_{\rm jt} R) = +i \frac{\beta_{\rm ex}}{\chi_{\rm ex}}. \tag{8}$$

Equation (7) describes the symmetric pinch mode of a slab jet, $C_{\rm as} = 0$ in equation (4), and equation (8) describes the asymmetric sinusoidal mode of a slab jet, $C_s = 0$ in equation (4).

We will assume that heating and cooling rates are of the form $H = \Lambda_H n^{\alpha_H} T^{\beta_H}$ and $C = \Lambda_C n^{\alpha_C} T^{\beta_C}$, respectively. Since we are only considering linear perturbations from the equilibrium state in this paper, this assumption requires simply that the heating and cooling functions be representable by power laws in the *neighborhood* of the equilibrium state. For the nonlinear simulations presented in Paper II, we will relax this assumption. The requirement that the initial configuration be in equilibrium, i.e., $H_0 - C_0 = 0$, means that

$$\Lambda_H n_0^{\alpha_H} T_0^{\beta_H} - \Lambda_C n_0^{\alpha_C} T_0^{\beta_C} = 0.$$

With these forms for the heating and cooling rates, F_p and F_ρ are of the form

$$F_p = \frac{\Gamma(\Gamma - 1)}{\rho_0 a^2} \boldsymbol{C}(\beta_C - \beta_H)$$

and

$$F_\rho = \frac{\Gamma - 1}{\rho_0 a^2} \boldsymbol{C}[(\beta_C - \beta_H) + (\alpha_H - \alpha_C)],$$

where $\boldsymbol{C} = \Lambda_C n_0^{\alpha_C} T_0^{\beta_C}$ ergs cm^{-3} s^{-1}. We will assume that the heating rate is independent of the temperature, i.e., $\beta_H = 0$, and is proportional to the density, i.e., $\alpha_H = 1$.

It is clear that the solutions to the dispersion relation will depend sensitively on the precise form of the cooling function we adopt, i.e., the values of α_C and β_C. Ultimately, we are interested in the stability of cooling jets in protostellar systems and Seyfert galaxies. Thus, we choose one cooling curve appropriate to interstellar gas and protostellar jets, and a second cooling curve appropriate to photoionized gas and Seyfert galaxies.

Numerical simulations indicate that jets remain relatively well collimated with small opening angles only if they are in pressure balance with the external medium. This appears to be the case for protostellar jets after possibly an initial rapid expansion phase (Ray et al. 1996). Numerical simulations (Norman, Winkler, & Smarr 1983; Cioffi & Blondin 1992) and simple physical arguments (Begelman & Cioffi 1989) show that light jets with densities less than the undisturbed external medium create large lobes of processed jet material, and that heavy jets create much smaller cocoons. Additionally, three-dimensional numerical simulations show that jets lighter than the surrounding medium are subject to filamentation and disruption by entrained material (Hardee, Clarke, & Howell 1995), where jets heavier than the surrounding medium are much more robust (Hardee & Clarke 1995). In particular, numerical simulations, e.g., Stone & Norman (1993a, 1993b, 1994), of propagating jets with nonequilibrium cooling show that jets of density comparable to or greater than the density of the undisturbed external medium and in pressure balance with that medium produce features similar to those seen in protostellar jets. In these simulations (also in adiabatic simulations of dense jets), the jet is surrounded by a cocoon of width a few times the jet diameter that is both hotter and less dense than the jet and hotter and less dense than the surrounding undisturbed external medium. The simulations also reveal a very low-ionization fraction in the colder jet material. Thus, for our

equilibrium jet configuration, we imagine a cold, dense protostellar jet of low-ionization fraction in equilibrium with a hotter, less dense cocoon. This hotter, less dense cocoon might be associated with observed line emission that may originate in an outflow mixing layer (e.g., HH 47 [Hartigan et al. 1993] and HH 110 [Noriega-Crespo et al. 1996]), and that comes from material with temperatures ranging from about 2500 to about 6000 K. Outside this layer, we might find the cold, poorly collimated molecular outflows that have been observed from some objects (e.g., HH 46/47 [Eislöffel et al. 1994] and HH 111 [Reipurth & Cernicharo 1995]). All of these regions must be in approximate pressure balance if the jets are to remain highly collimated.

In order to maximize the possible effects of cooling, we choose a cooling function that has $\beta_C = 0.5$ and $\alpha_C = 2$, and we choose $\Lambda_C^{ex} = 1.5 \times 10^{-24}$ when $10^4 \leq T \leq 2 \times 10^5$ (e.g., Bertschinger 1986) for the cooling in a hot cocoon around the denser jet. In the colder jet fluid, we choose $\Lambda_C^{jt} = 3.0 \times 10^{-28}$, corresponding to an assumed ionization fraction $n_e/n \leq 0.001$ (e.g., Dalgarno & McCray 1972; Spitzer 1978, p. 142). This discontinuous cooling function adequately mimics the Dalgarno & McCray cooling curve (see Fig. 1*a*) for low-ionization fractions in fluid below 10^4 K. For ionization fractions $0.001 \leq n_e/n \leq 0.1$, $\Lambda_C^{jt} \approx 9.5 \times 10^{-27}(n_e/n)^{0.5}$. This choice will serve to illustrate the possible effects of cooling on the stability of a cold, dense protostellar jet propagating within a hotter, less dense, slowly moving cocoon and in which cooling is a shallow function of temperature (e.g., proportional to $T^{0.5}$) in each medium.

For purposes of calculation, we will consider a jet of radius $R = 2.5 \times 10^{15}$ cm with number density $n_{jt} = 600$ cm^{-3}, temperature $T = 10^3$ K, and sound speed $a_{jt} = 3.73 \times 10^5$ cm s^{-1} (similar to parameters chosen for propagating jet simulations). The external number density is assumed to be 1/10 the jet number density, i.e., $n_{ex} = 60$ cm^{-3}, the external medium has a temperature of $T = 10^4$ K, and the external sound speed is $a_{ex} = 1.18 \times 10^6$ cm s^{-1}. With this choice of parameters,

$$\begin{Bmatrix} F_p^{ex} \\ F_p^{jt} \end{Bmatrix} = \frac{5}{9\rho_0 a^2} \Lambda_C n_0^2 T_0^{0.5} = \begin{Bmatrix} 2.16 \times 10^{-9} \text{ s}^{-1} \\ 1.37 \times 10^{-11} \text{ s}^{-1} \end{Bmatrix},$$

and

$$\begin{Bmatrix} F_\rho^{ex} \\ F_\rho^{jt} \end{Bmatrix} = -\frac{1}{3\rho_0 a^2} \Lambda_C n_0^2 T_0^{0.5} = \begin{Bmatrix} -1.29 \times 10^{-9} \text{ s}^{-1} \\ -0.82 \times 10^{-11} \text{ s}^{-1} \end{Bmatrix}.$$

An alternative cooling function such as that used by MacDonald & Bailey (1981), which is of the form $C = n_e n_H L(T)$, where n_e and n_H are the free electron and total hydrogen number densities, respectively, is appropriate to Seyfert galaxies. For $10^6 < T < 10^8$ K, $L(T)$ is given by the steady state cooling curve of Raymond, Cox, & Smith (1976), but with reduced iron

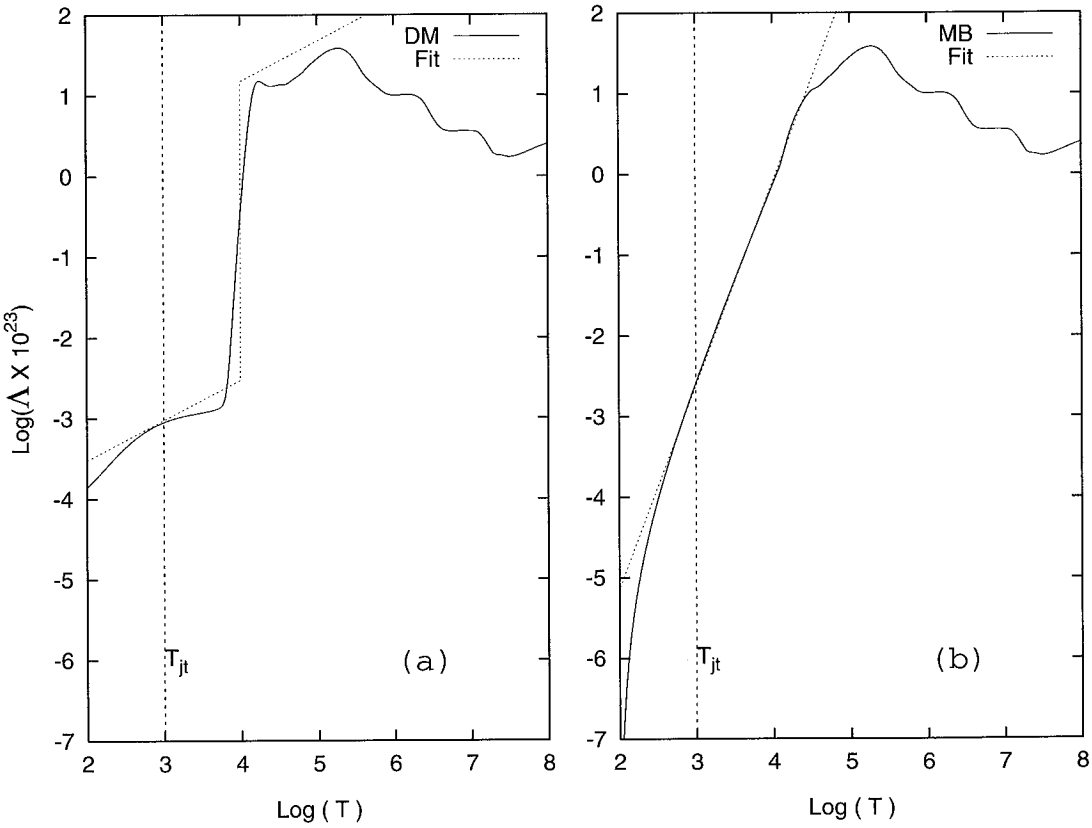

FIG. 1.—Per particle cooling rates for (*a*) the DM cooling curve and (*b*) the MB cooling curve. The dotted lines indicate the power-law fits used in the linear analysis.

abundance (see MacDonald & Bailey 1981). For $10^4 < T < 10^6$ K, $L(T)$ is given by the time-dependent isochoric cooling curve of Shapiro & Moore (1976). Below 10^4 K, the Shapiro & Moore curve was extrapolated so that $L(T) \to 0$ as $T \to 10^2$. For the purposes of our linear analysis, we can fit the MacDonald & Bailey (1981) cooling curve as $\boldsymbol{C} = \Lambda_C n_0^{\alpha_C} T_0^{\beta_C}$ ergs cm^{-3} s^{-1}, where $\Lambda_C = 1.5 \times 10^{-34}$, $\beta_C \approx 2.53$, and $\alpha_C = 2$. Figure 1*b* demonstrates that this fit is satisfactory over a broad temperature range. While this cooling curve is more relevant to jets in galaxies, in this paper we use the same protostellar jet parameters chosen for the Dalgarno & McCray cooling curve. This cooling curve serves to illustrate the effect of cooling as a steep function of temperature (e.g., proportional to $T^{2.53}$) in each medium, and it also probes the effect of an order of magnitude reduction in external cooling while maintaining the internal cooling rate. With protostellar jet parameters,

$$\begin{Bmatrix} F_p^{\rm ex} \\ F_p^{\rm jt} \end{Bmatrix} \approx \frac{25}{9\rho_0 a^2} \Lambda_C n_0^2 T_0^{2.53} = \begin{Bmatrix} 1.46 \times 10^{-10}\ {\rm s}^{-1} \\ 4.30 \times 10^{-11}\ {\rm s}^{-1} \end{Bmatrix},$$

and

$$\begin{Bmatrix} F_\rho^{\rm ex} \\ F_\rho^{\rm jt} \end{Bmatrix} \approx \frac{1}{\rho_0 a^2} \Lambda_C n_0^2 T_0^{2.53} = \begin{Bmatrix} 5.24 \times 10^{-11}\ {\rm s}^{-1} \\ 1.54 \times 10^{-11}\ {\rm s}^{-1} \end{Bmatrix}.$$

The most important differences in jet stability properties between Dalgarno & McCray (DM) cooling and MacDonald & Bailey (MB) cooling will be seen to arise from the change in sign of F_ρ. The positive value of F_ρ for MB cooling is a consequence of the steeper temperature dependence of the MB cooling function. Positive values of F_ρ occur when $(\beta_C - \beta_H) + (\alpha_H - \alpha_C) > 0$. For our choice of heating rate depending linearly on the density and of cooling rate depending on the density squared, $F_\rho > 0$ when $\beta_C > 1$. We will also investigate the effect of varying Λ_C to ascertain the effect of overestimates or underestimates of the cooling enforced by our simple, sharp discontinuity between jet and external medium. The assumed equilibrium state requires a considerably different heating rate in the jet and in the external material. There probably are not physical sources that would lead to such different heating rates, but we must make this choice to establish the equilibrium state.

3. APPROXIMATE SOLUTIONS TO THE DISPERSION RELATIONS

3.1. *Low-Frequency Limit*

3.1.1. *Pinch Mode Surface Wave and the Cooling Mode*

The symmetric pinch mode dispersion relation admits a surface (fundamental) wave and multiple body (reflection) wave solutions. In the low-frequency limit, the pinch mode surface wave solution is found from equation (7), with $\tan(\beta_{\rm jt} R) \approx \beta_{\rm jt} R \ll 1$, and is given approximately by

$$\frac{\omega}{k_z} \approx u \pm \frac{\cos(\theta - \phi_{\rm jt})}{\cos\theta}\left[2\left(1 - i\frac{u^2X^2/\eta}{a_{\rm jt}^2/Q_{\rm jt} + V_{\rm A,jt}^2}\frac{\omega R}{u}\right)\right]^{-1/2}\left\{\left(V_{\rm A,jt}^2 + \frac{V_{\rm A,jt}^2 a_{\rm jt}^2/Q_{\rm jt}}{a_{\rm jt}^2/Q_{\rm jt} + V_{\rm A,jt}^2} - \frac{u^2X^2/\eta}{\cos^2(\theta - \phi_{\rm jt})}\frac{\omega R}{u}\right)\right.$$
$$\pm\left[\left(V_{\rm A,jt}^2 + \frac{V_{\rm A,jt}^2 a_{\rm jt}^2/Q_{\rm jt}}{a_{\rm jt}^2/Q_{\rm jt} + V_{\rm A,jt}^2} - \frac{u^2X^2/\eta}{\cos^2(\theta - \phi_{\rm jt})}\frac{\omega R}{u}\right)^2 - 4\left(1 - \frac{u^2X^2/\eta}{a_{\rm jt}^2/Q_{\rm jt} + V_{\rm A,jt}^2}\frac{\omega R}{u}\right)\right.$$
$$\left.\left.\times\left[\left(\frac{V_{\rm A,jt}^4 a_{\rm jt}^2/Q_{\rm jt}}{a_{\rm jt}^2/Q_{\rm jt} + V_{\rm A,jt}^2} - \frac{X^2u^2V_{\rm A,jt}^2 a_{\rm jt}^2/Q_{\rm jt}}{\eta(a_{\rm jt}^2/Q_{\rm jt} + V_{\rm A,jt}^2)\cos^2(\theta - \phi_{\rm jt})}\frac{\omega R}{u}\right)\right]^{1/2}\right\}^{1/2}, \quad (9)$$

where

$$X^2 \approx i\left\{1 - \left[\left(\frac{k_z V_{\rm A,ex}}{\omega}\right)^2 \frac{\cos^2(\theta - \phi_{\rm ex})}{\cos^2\theta}\right]\right\}\left\{\frac{M_{\rm ms,ex}^2}{1 - (M_{\rm ms,ex}/M_{\rm ex}M_{\rm A,ex})^2(k_z u/\omega)^2[\cos^2(\theta - \phi_{\rm ex})/\cos^2\theta]} - \left(\frac{ku}{\omega}\right)^2\right\}^{-1/2}$$

contains all the parameters associated with the external medium. The Alfvén Mach number is defined as $M_{\rm A,ex} \equiv u/V_{\rm A,ex}$, and $M_{\rm ex} \equiv Q_{\rm ex}^{1/2} u/a_{\rm ex}$ and $M_{\rm ms,ex} \equiv u/(a_{\rm ex}^2/Q_{\rm ex} + V_{\rm A,ex}^2)^{1/2}$ become *complex* sonic and *complex* magnetosonic Mach numbers, respectively. The solutions given by equation (9) are related to fast (the plus sign in the radical) and slow (the minus sign in the radical) magnetosonic waves propagating with $(u+)$ and against $(u-)$ the jet flow speed u, but strongly modified by the jet-external medium interface, and further modified by the cooling rates through $Q_{\rm jt}$ and $Q_{\rm ex}$. In the adiabatic limit, $Q_{\rm jt} = Q_{\rm ex} = 1$, the unstable growing solution is associated with the backward-moving (in the reference frame of the jet fluid) slow surface wave. A second solution arises from equation (7), when $(\omega - k\cos\theta u) + iF_\rho^{\rm jt} \approx 0$ and $Q_{\rm jt} \gg 1$. When $(1 - \omega/k_z u)^2 \gg V_{\rm A,jt}^2 \cos^2(\theta - \phi_{\rm jt})/u^2\cos^2\theta$, an approximate solution is given by

$$k_z u \approx \omega + \frac{i}{1 + V_{\rm A,jt}^2/a_{\rm jt}^2}\left(F_\rho^{\rm jt} + \frac{V_{\rm A,jt}^2}{a_{\rm jt}^2}F_p^{\rm jt}\right), \quad (10)$$

and there is a plateau in the imaginary part of the wavenumber at low frequencies. This approximation indicates the existence of a cooling mode that does not exist in the adiabatic limit, and this mode is growing if the imaginary part is negative and damped if the imaginary part is positive. For our cooling functions with $F_p^{\rm jt} > 0$, growth or damping depends on the sign of $F_\rho^{\rm jt}$, and when $F_\rho^{\rm jt} + (V_{\rm A,jt}^2/a_{\rm jt}^2)F_p^{\rm jt} < 0$, the cooling mode is growing.

3.1.2. *Sinusoidal Mode Surface Wave*

The asymmetric sinusoidal mode dispersion relation admits a surface (fundamental) wave and multiple body (reflection) wave solutions. In the low-frequency limit, the sinusoidal mode surface wave solution is found from equation (8), with $\cot(\beta_{jt}R) \approx 1/\beta_{jt}R$, and is given approximately by (Hardee et al. 1992, hereafter HCNS)

$$\frac{k_z u}{\omega} \approx \left\{1\Big/\left[1 - \frac{V_{A,jt}^2}{u^2}\frac{\cos^2(\theta - \phi_{jt})}{\cos^2\theta}\right]\right\}\left[1 \pm i\left\{\left[1 - \frac{V_{A,jt}^2}{u^2}\frac{\cos^2(\theta - \phi_{jt})}{\cos^2\theta}\right]\frac{X^2/\eta}{\omega R/u} - \frac{V_{A,jt}^2}{u^2}\frac{\cos^2(\theta - \phi_{jt})}{\cos^2\theta}\right\}^{1/2}\right]. \quad (11)$$

For supermagnetosonic jets, growing waves correspond to the solution with $\mathrm{Re}[X^2] > 1$. The jet-to-external medium density ratio is $\eta \equiv \rho_{jt}/\rho_{ex}$, and in the dense jet limit ($\eta \to \infty$), equation (11) becomes $\omega/k \approx u\cos\theta \pm V_{A,jt}\cos(\theta - \phi_{jt})$. The sinusoidal surface wave is therefore related to Alfvén waves propagating with and against the jet flow speed u, but strongly modified by the jet/external medium interface. The unstable growing solution is associated with the backward-moving (in the jet reference frame) surface wave. This surface wave is modified by cooling in the external medium through the dependence of X on Q_{ex}, but unlike the case for the symmetric pinch mode, no additional cooling mode solution arises from Q_{jt}.

3.1.3. *Body Waves*

The symmetric pinch mode body wave solutions in the low-frequency limit are (Hardee 1995)

$$k_z R \approx \left(m - \frac{1}{2}\right)\pi\left\{\frac{M_{ms,jt}^2}{1 - (M_{ms,jt}/M_{jt}M_{A,jt})^2[\cos^2(\theta - \phi_{jt})/\cos^2\theta]} - \frac{1}{\cos^2\theta}\right\}^{-1/2}, \quad (12)$$

where $m \geq 1$ is an integer, $M_{A,jt} \equiv u/V_{A,jt}$ is the Alfvén Mach number, and $M_{jt} \equiv Q_{jt}^{1/2}u/a_{jt}$ and $M_{ms,jt} \equiv u/(a_{jt}^2/Q_{jt} + V_{A,jt}^2)^{1/2}$ are now *complex* sonic and magnetosonic Mach numbers, respectively. The asymmetric sinusoidal mode body wave solutions in the low-frequency limit are given by (HCNS)

$$k_z R \approx m\pi\left\{\frac{M_{ms,jt}^2}{1 - (M_{ms,jt}/M_{jt}M_{A,jt})^2[\cos^2(\theta - \phi_{jt})/\cos^2\theta]} - \frac{1}{\cos^2\theta}\right\}^{-1/2}, \quad (13)$$

where $m \geq 1$ is an integer. The low-frequency form for the body modes indicates that these modes exist, provided the expression in braces in equations (12) and (13) has a real part. In the adiabatic limit for the case where the magnetic field and wavevector are aligned with the flow, i.e., $\cos^2(\theta - \phi_{jt}) = 1$ and $\cos^2\theta = 1$, the typical behavior of the denominator (see Fig. 1 in HCNS) shows that the body waves exist if the jet speed exceeds the fast magnetosonic speed, or if the jet speed is slightly below the slow magnetosonic speed. Equations (12) and (13) indicate that the body wave solutions are purely real in the low-frequency limit on the adiabatic jet. However, the addition of cooling in the jet fluid implies a complex value for Q_{jt}, and thus a complex value for $M_{ms,jt}$ and M_{jt}. As a result, body wave solutions should be complex: the numerical solution of the dispersion relation shows that these waves are damped at low frequencies on the cooling jet.

3.2. *Maximum Growth Rate*

With the exception of the pinch mode surface wave, which in general has a broad plateau in the growth rate, all body waves and the sinusoidal mode surface wave have a relatively sharp maximum in the growth rate when the jet is supermagnetosonic and adiabatic (cf. HCNS). In the supermagnetosonic limit, we anticipate that a maximum in the growth rate will be achieved when

$$\frac{\omega_m^* R}{(a_{ex}^2/Q_{ex}^{1/2} + V_{A,ex}^2)^{1/2}} \approx m\pi + \left(\frac{\pi}{2}\right)_{as}, \qquad v_{ph}^* \approx \frac{M_{ms,jt}/M_{ms,ex}}{1 + M_{ms,jt}/M_{ms,ex}}u, \qquad \lambda_m^* \approx \frac{2\pi}{m\pi + (\pi/2)_{as}}\frac{M_{ms,jt}}{1 + M_{ms,jt}/M_{ms,ex}}R, \quad (14)$$

where $m = 0$ gives the sinusoidal mode surface wave, $m \geq 1$ gives the pinch and sinusoidal mode body waves, and $(\pi/2)_{as}$ is added for the sinusoidal mode. In equations (14), ω_m^*, v_{ph}^*, and λ_m^* are real quantities, and only the real part of complex quantities should be used. It is clear that the effects of cooling can modify these expressions through the value of Q. For example, $Q_{ex} > 1$ will decrease the frequency at which maximum growth occurs; $Q_{ex} < 1$ will effectively increase the sound speed and, in the absence of magnetic fields, will result in an increase in the frequency at which maximum growth occurs. Note that the frequency at which maximum growth occurs should be independent of the internal cooling rate, although the phase velocity and wavelength are dependent on the internal cooling rate through $M_{ms,jt}$. With the exception of the pinch mode surface wave, the maximum spatial growth rate of these waves is approximately given by

$$k_I^* \approx -(2M_{ms,jt}R)^{-1}\ln\left[4\frac{\omega_m^* R}{(a_{ex}^2/Q_{ex} + V_{A,ex}^2)^{1/2}}\right], \quad (15)$$

where the real part of complex quantities must be used. When the adiabatic jet is subsonic in the absence of magnetic fields or transmagnetosonic but super-Alfvénic in the presence of magnetic fields, the growth rate of both symmetric pinch and asymmetric sinusoidal surface waves has no maximum and increases proportional to the frequency. If $Q_{ex} < 1$, the sonic or magnetosonic Mach numbers might be reduced sufficiently to modify the transition point between supermagnetosonic and transmagnetosonic regimes.

3.3. *High-Frequency Limit*

3.3.1. *Symmetric and Asymmetric Cooling Modes*

In the supermagnetosonic limit when $\omega \to \infty$, a symmetric pinch mode solution can be found from equation (7) when $(\omega - k_z u) \approx 0$ and $Q_{jt} \gg 1$, which is given by

$$k_z u \approx \omega + iF_\rho^{jt} . \tag{16}$$

Growth or damping will be determined by the sign of F_ρ^{jt}. At high frequencies, a cooling mode solution can arise from equations (7) and (8) when $\beta_{jt} R \to i\infty$ and $i \tan (i\infty) \to -i \cot (i\infty) \to -1$. In this case, both symmetric and asymmetric dispersion relations are given approximately by $\chi_{jt} \beta_{ex} \approx -\chi_{ex} \beta_{jt}$. In the supermagnetosonic limit for which χ_{ex} and χ_{jt} take on their purely fluid forms, and for which $\beta_{jt} \approx [(\omega - k_z u)^2/(a_{jt}^2/Q_{jt} + V_{A,jt}^2)]^{1/2}$ and $\beta_{ex} \approx [\omega^2/(a_{ex}^2/Q_{ex} + V_{A,ex}^2)]^{1/2}$, an approximate solution for the symmetric and asymmetric mode surface wave is given by

$$\frac{k_z u}{\omega} \approx 1 + \frac{1}{\eta^{1/2}} \left(\frac{Q_{jt}}{Q_{ex}}\right)^{1/2} \left[\frac{1 + (V_{A,ex}^2/a_{ex}^2) Q_{ex}}{1 + (V_{A,jt}^2/a_{jt}^2) Q_{jt}}\right]^{1/2} . \tag{17}$$

It is obvious that the solution in the adiabatic limit ($Q_{jt} = Q_{ex} = 1$) is purely real. In the high-frequency limit, where $Q_{ex} \approx 1 + i(F_p^{ex} - F_\rho^{ex})/\omega$ and $(\omega - k_z u) \neq 0$ so that $Q_{jt} \approx 1 + i(F_p^{jt} - F_\rho^{jt})/(\omega - k_z u)$, and if $(V_A^2/a^2) Q \ll 1$, it follows that

$$\frac{k_z u}{\omega} \approx 1 + \frac{1}{\eta^{1/2}} \left[\frac{1 + (V_{A,ex}^2/a_{ex}^2)}{1 + (V_{A,jt}^2/a_{jt}^2)}\right]^{1/2} - \frac{i}{2} \left[\frac{1}{1 + (V_{A,jt}^2/a_{jt}^2)}\right]^{1/2} \left[\left\{\frac{F_p^{ex} - F_\rho^{ex}}{[1 + (V_{A,ex}^2/a_{ex}^2)]\omega}\right\} \Big/ \eta^{1/2} + \left\{\frac{F_p^{jt} - F_\rho^{jt}}{[1 + (V_{A,jt}^2/a_{jt}^2)]^{1/2}\omega}\right\}\right] , \tag{18}$$

where we have used $(\omega - k_z u) \approx -[(1 + V_{A,ex}^2/a_{ex}^2)/\eta(1 + V_{A,jt}^2/a_{jt}^2)]^{1/2}$ in Q_{jt}. Another possibility is that $(V_{A,ex}^2/a_{ex}^2)^2 Q_{ex} \ll 1$ but $(V_{A,jt}^2/a_{jt}^2) Q_{jt} \gg 1$, in which case

$$\frac{k_z u}{\omega} \approx 1 + \frac{a_{jt}}{\eta^{1/2} V_{A,jt}} \left(\frac{1}{Q_{ex}}\right)^{1/2} \approx 1 + \frac{a_{jt}}{\eta^{1/2} V_{A,jt}} - i \frac{a_{jt}}{2\eta^{1/2} V_{A,jt}} \left(\frac{F_p^{ex} - F_\rho^{ex}}{\omega}\right) . \tag{19}$$

Both of these cases indicate the potential for growth associated with cooling, provided $F_p - F_\rho > 0$. Note that as $\omega \to \infty$, $Q_{ex} \to 1$ and $Q_{jt} \to 1$ in equation (17) so that these waves should approach the adiabatic high-frequency limiting form in which the growth rate decreases to zero.

3.3.2. *Symmetric and Asymmetric Mode Body Waves*

In the high-frequency limit, the real part of the usual adiabatic solutions to the symmetric and asymmetric dispersion relations, but now modified by the effect of cooling in the jet fluid, is given by (e.g., HCNS)

$$\frac{\omega}{k} \approx u \cos\theta \pm \left[\frac{1}{2}\left(\frac{a_{jt}^2}{Q_{jt}} + V_{A,jt}^2\right)\left\{1 \pm \left[1 - \frac{4V_{A,jt}^2 a_{jt}^2/Q_{jt}}{(a_{jt}^2/Q_{jt} + V_{A,jt}^2)^2} \cos^2(\theta - \phi_{jt})\right]^{1/2}\right\}\right]^{1/2} . \tag{20}$$

Equation (20) describes fast, $\omega/k \approx u \pm \max(V_{A,jt}, a_{jt})$, and slow, $\omega/k \approx u \pm \min(V_{A,jt}, a_{jt})$, magnetosonic waves, and unstable growing solutions are associated with the backward-moving, fast magnetosonic wave. With the exception of the cooling modes, the real part of all other symmetric and asymmetric mode waves is described by equation (20), and the growth rate is found numerically to approach zero as the frequency increases.

4. NUMERICAL SOLUTION OF THE DISPERSION RELATIONS

4.1. *Fluid Jet*

We have solved the dispersion relations in equations (7) and (8) numerically by using root-finding techniques over a wide range of perturbation frequencies. Figures 2 and 3 provide a comparison between the resulting solutions computed for an adiabatic jet, a nonadiabatic jet with DM-type cooling, and a nonadiabatic jet with MB-type cooling. Figure 2 gives the results for a $M_{ex} = 5.0$ jet with speed $u = 5.9 \times 10^6$ cm s^{-1}, while Figure 3 gives the result for a $M_{ex} = 20.0$ jet with speed $u = 23.6 \times 10^6$ cm s^{-1}. Within each panel of each figure, the surface and first three-body waves associated with symmetric pinch (top panels) or asymmetric sinusoidal (bottom panels) modes are plotted. Only those waves that have some frequency range exhibiting growth are shown. Damping rates associated with these waves are not shown in order to reduce complexity. In general, waves are purely real where no imaginary part is shown for the adiabatic case, and waves are damped where no imaginary part is shown when cooling is important. Note that from a comparison of Figures 2 and 3, in all cases the principal difference between Mach 5 and Mach 20 jets is a shift in the dimensionless frequency, $\omega^* R/u$, at which maximum growth rate peaks occur, and a reduction in the maximum growth rate approximately inversely proportional to the Mach number as indicated by equations (14) and (15). DM-type cooling leads to enhanced growth rates and growing cooling modes, whereas MB-type cooling leads to similar or reduced growth rates and damped cooling modes when compared with adiabatic growth rates. In the following sections, we discuss the results presented in Figures 2 and 3 in more detail.

4.1.1. *Symmetric Mode*

A growing cooling mode (S2) exists in the presence of DM-type cooling. In the presence of DM-type cooling, S2 has a constant growth rate of $k_I R \approx F_\rho^{jt} R/u$ at the lowest frequencies, in accordance with equation (10), and at higher frequencies,

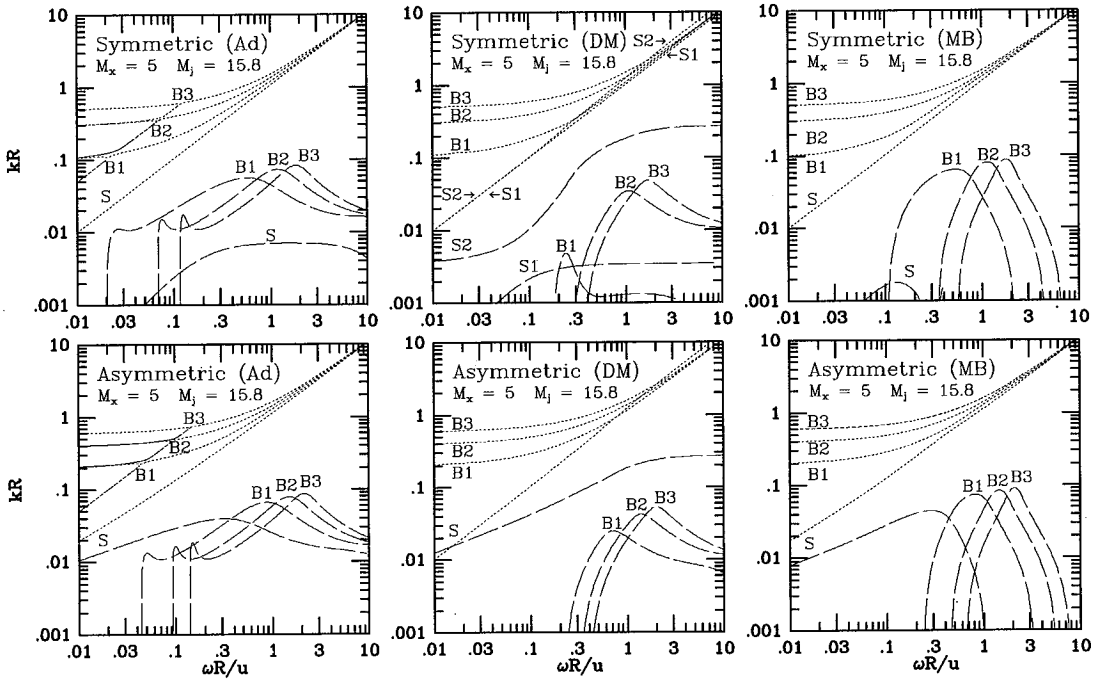

FIG. 2.—Surface (S) and first three-body wave (B) solutions to the symmetric and asymmetric dispersion relations for Mach 5 adiabatic and radiatively cooled jets for the DM cooling function and the MB cooling function. The dashed lines give the imaginary part of the wavenumber.

the growth rate increases to $k_I R \approx (4/3\eta^{1/2})F_\rho^{\rm ex} R/u$ as predicted by equation (18). The growth rate of S2 is considerably greater than the growth rate of the surface mode (S) on the adiabatic jet or the growth rate of the equivalent surface mode (S1) on the cooling jet. The expected decrease in the growth rate of S2 at the highest frequencies is visible in the panels for the Mach 20 jet (Fig. 4) at frequencies $\omega R/u > 9$. It should be noted that S2 exists in the presence of MB-type cooling but is heavily damped, and thus it is not plotted in the figures. The damping of S2 in the presence of MB-type cooling is a result of the fact that $F_\rho^{\rm jt} + (V_{{\rm A,jt}}^2/a_{\rm jt}^2)F_p^{\rm jt} > 0$ in equation (10) and $F_\rho^{\rm jt} > 0$ in equation (16), although the damping rate is somewhat higher than predicted by these approximations. In the presence of DM-type cooling the growth rate of S1 rises at low frequencies like the adiabatic case but asymptotes to a growth rate of $k_I R \approx F_\rho^{\rm jt} R/u$ at higher frequencies in accordance with

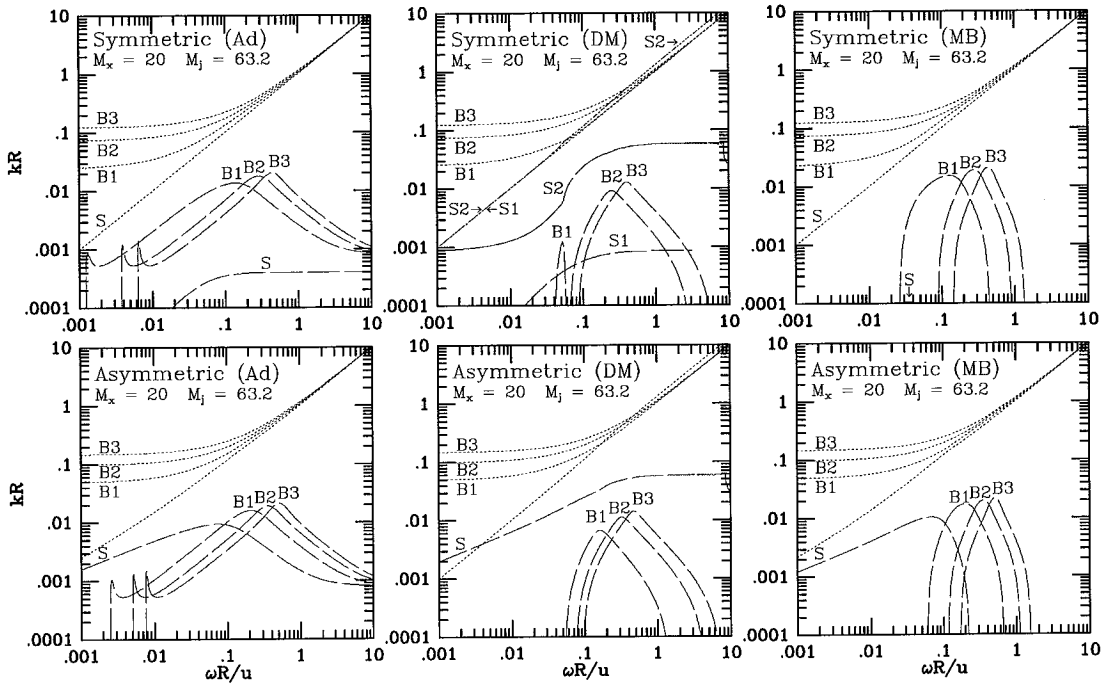

FIG. 3.—Surface (S) and first three-body wave (B) solutions to the symmetric and asymmetric dispersion relations for Mach 20 adiabatic and radiatively cooled jets for the DM cooling function and the MB cooling function. The dashed lines give the imaginary part of the wavenumber.

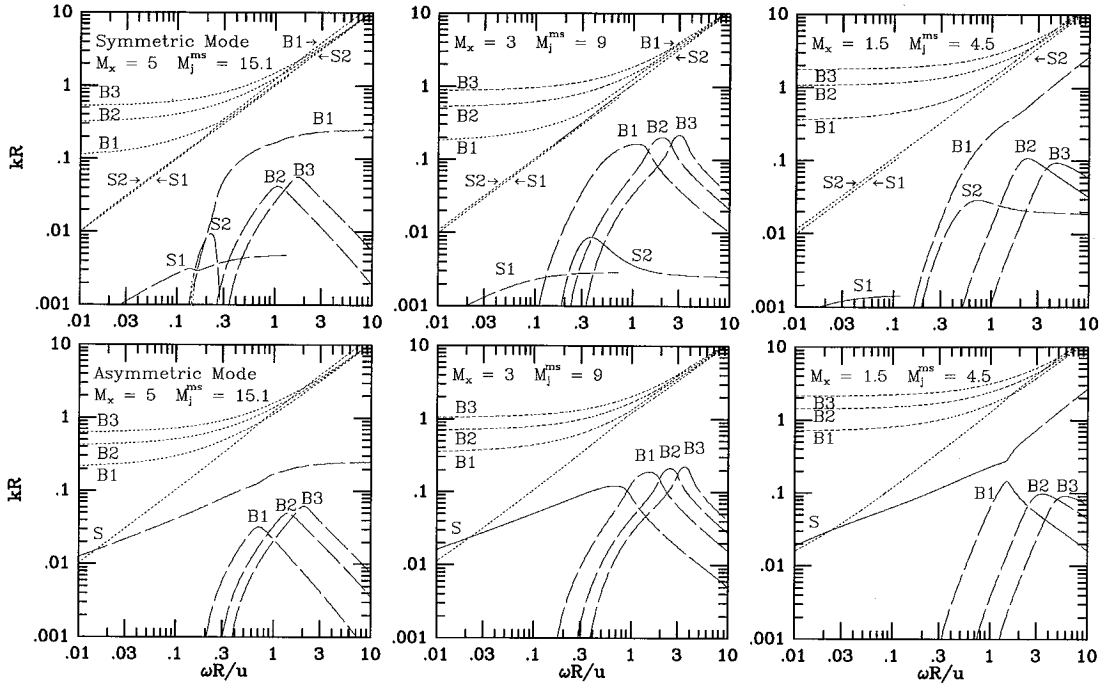

FIG. 4.—Surface (S) and first three-body wave (B) solutions to the symmetric and asymmetric dispersion relations for magnetized adiabatic and radiatively cooled jets for the DM cooling function.

equation (16). This value is below the comparable growth rate on the adiabatic jet for $M_{ex} = 5.0$ but above the growth rate on the adiabatic jet for $M_{ex} = 20.0$. Thus, while the maximum growth rate of the symmetric surface mode (S) on the adiabatic jet decreases approximately inversely proportional to the square of the Mach number, the maximum growth rate of the symmetric surface mode (S1) on the DM cooling jet decreases approximately inversely proportional to the Mach number. The surface wave S1 has had its growth rate severely reduced in the presence of MB-type cooling. Note that there is a large reduction in the growth rate of the first body wave (B1) in the presence of DM-type cooling, indicating a strong coupling between the surface waves and the first body wave. In general, the growth rates of the symmetric body waves are reduced by the inclusion of cooling, and the maximum growth rate is shifted to a lower frequency. The lowest order body waves are affected more than the higher order body waves. At the lower frequencies, the body waves remain complex and are strongly damped for both DM-type cooling and MB-type cooling. At the higher frequencies, the body waves are again heavily damped in the presence of MB-type cooling.

The effect of varying the external and internal cooling rates for DM-type cooling was studied. In general, the growth rate of S2 is increased as the external cooling rate is increased, with the most profound effects occurring at high frequencies. On the other hand, it was found that a reduction of the external cooling rate by a factor 2 less than that used in Figure 2 eliminates the high-frequency plateau. Internal cooling is responsible for the low-frequency plateau in the growth rate of S2, and the low-frequency growth rate increases as the internal cooling rate increases. In general, the high-frequency growth rate is suppressed by internal cooling in the absence of external cooling. Given these results, it is possible that the high growth rate of S2 at high frequencies that is seen in Figures 2 and 3 is relatively sensitive to the choice of internal and external cooling rates. On the other hand, the low-frequency behavior shows only the modest changes predicted by the analytical approximations for S1 and S2 as internal and external cooling rates vary.

The growth rate of the first symmetric body wave (B1) is affected greatly by the external cooling rate at low and high frequencies. At low frequencies, the growth rate is suppressed as the cooling rate increases. At high frequencies, the growth rate increases initially as the cooling rate increases, but for a DM cooling rate twice that used in Figure 2, the growth rate is greatly decreased below the adiabatic values. This result implies that the presently calculated growth rate for the first body wave shown in Figures 2 and 3 is relatively sensitive to the choice of the external cooling rate. In general, the second body wave (B2) also shows a decrease in the growth rate as the external cooling rate is increased, with the exception of the maximum growth rate, which first increases and then decreases as the external cooling rate is increased further. While change in the external cooling rate can produce varying large effects in the growth rate of these body waves, we find that an increase in the internal cooling rate results in a predictable decrease in growth rates of the body waves at frequencies above and below the maximally growing frequency but has little effect on the maximum growth rate. This result is in agreement with equations (14) and (15), which predict that the maximally growing frequency and maximum growth rate are sensitive to the external cooling rate through Q_{ex} only.

4.1.2. *Asymmetric Mode*

The asymmetric dispersion relation admits no cooling mode at low frequencies in addition to the surface wave (S). However, the growth rate of S is increased at all frequencies relative to its growth rate on the adiabatic jet. The increase in

growth rate at low frequencies results from cooling in the external medium via Q_{ex} in equation (11) and is about a factor 2 larger at the adiabatic maximum for DM-type cooling, but only about 20% larger at the adiabatic maximum for MB-type cooling. The growth rate increases to $k_I R \approx (4/3\eta^{1/2})F_\rho^{ex} R/u$ at the higher frequencies for DM-type cooling, and at the higher frequencies, the growth rate plateau is identical to that of the symmetric cooling mode S2 as predicted by equation (17). The expected decrease in the growth rate at the highest frequencies is visible in Figure 3 for the Mach 20 jet at frequencies $\omega R/u > 9$. In the presence of MB-type cooling, the surface mode is strongly damped above the maximally growing frequency. The growth rate of the asymmetric mode first body wave is reduced relative to the adiabatic jet but not as severely as the symmetric mode first body wave. In general, the growth rates of the body waves are reduced by the inclusion of cooling, and the maximum growth rate is shifted to a lower frequency. The lowest order body waves are affected more than the higher order body waves. At the lower frequencies, the body waves are strongly damped, and they are strongly damped at the higher frequencies for MB-type cooling also. With the exception of the first body wave, asymmetric and symmetric mode body waves respond similarly to the effect of cooling.

The effect of varying the external and internal cooling rates for DM-type cooling showed that increasing the external cooling rate raises the growth rate of the asymmetric surface wave at low frequencies. In general, the growth rate is increased as the external cooling rate is increased, with the most profound effects occurring at high frequencies, just as was found to be the case for the symmetric mode S2. On the other hand, it was found that a reduction of the external cooling rate by a factor 2 less than that used in Figure 2 eliminates the high-frequency plateau evident in Figures 2 and 3. Increasing the internal cooling rate provides a predictable, modest decrease in the high-frequency growth rate, and our results appear to be insensitive to the value of the internal cooling rate.

In general, both first (B1) and second (B2) asymmetric mode body waves show a decrease in the growth rate as the external cooling rate is increased relative to the adiabatic jet, with the exception of the maximum growth rate, which first increases and then decreases as the external cooling rate is increased further, and with behavior like the second symmetric mode body wave. We note that no plateau appears in the high-frequency growth rate of the first asymmetric mode body wave (B1) and that this is unlike the first symmetric mode body wave. While change in the external cooling rate can produce varying large effects in the growth rate of these body waves, we find that an increase in the internal cooling rate results in a predictable decrease in growth rates of the body waves at frequencies above and below the maximally growing frequency but has little effect on the maximum growth rate. Thus, symmetric second and higher order body waves, and asymmetric mode first and higher order body waves, respond similarly to the effects of cooling.

4.2. *Magnetized Jet*

The effect of magnetic fields has been examined for a jet with DM-type cooling, with magnetic field parallel to the flow, and with equal thermal and magnetic pressures in the jet. For equal thermal and magnetic pressures, the jet Alfvén speed is greater than the jet sound speed with $V_{A,jt} \approx 1.2a_{jt}$. Solutions to the symmetric and asymmetric dispersion relations for the surface and first three body waves are shown in Figure 4 for jets with external sonic Mach numbers of 5.0, 3.0, and 1.5 and internal magnetosonic Mach numbers $M_{ms,jt} = 15.1$, 9.0, and 4.5, respectively. For these cases, the jet velocity was held constant, and the external medium temperature was raised to reduce the external Mach number and to reduce the internal Mach numbers by raising the jet temperature and magnetic field strength to maintain pressure balance. These three cases reveal the most important effects of the magnetic field from the supermagnetosonic into the transmagnetosonic regime. In all cases, the jet remains supersonic and super-Alfvénic internally. For the Mach 5 magnetized jet, there are differences in the detailed structure of the solutions for surface and body waves when compared with the unmagnetized jet, but the only significant differences lie in the disappearance of the low-frequency plateau associated with the symmetric cooling mode S2, and the fact that the high-frequency growth rate plateau resulting from cooling now appears to arise from the first symmetric mode body wave (B1) and not from S2 as in the unmagnetized case. The disappearance of the low-frequency plateau has occurred as predicted by equation (10) because $F_\rho^{jt} + (V_{A,jt}^2/a_{jt}^2)F_p^{jt} > 0$. While our numerical routines are unable to follow S1 up to the highest frequencies, we have nearly reached a maximum plateau growth rate $k_I R \approx 1.4F_\rho^{jt} R/u$ that is about 40% larger than predicted by equation (16) and that is somewhat greater than the maximum growth rate on a comparable Mach 5 adiabatic jet. Because the highest growth rates are not affected significantly by the magnetic field, we conclude that even a relatively strong magnetic field does not have a large effect on the stability properties of the cooling jet in the linear limit. Note that this also proves to be the case for the adiabatic jet in the supermagnetosonic limit but that the development of growing perturbations has been found to be affected in the nonlinear limit by magnetic tension (HCNS; Hardee & Clarke 1995).

As the jet Mach number is decreased to 3, we find that the high-frequency cooling–driven plateau in the growth rate is eliminated, and in general the growth rates associated with pinch mode surface waves S1 and S2 are reduced. While our numerical routines are unable to follow S1 up to the highest frequencies, we have nearly reached a maximum plateau growth rate $k_I R \approx 0.9F_\rho^{jt} R/u$ that now proves to be somewhat smaller than the maximum growth rate on a comparable adiabatic jet. In general, the maximum growth rates of the asymmetric surface wave and of the body waves are somewhat greater than on the comparable adiabatic jet, but the structure of the solutions to the dispersion relations is quite similar. As the jet Mach number is further decreased to 1.5, the solutions to the dispersion relations display a typical transmagnetosonic structure, with the exception of the symmetric cooling mode S2 and some difference in the maximum growth rate of S1 ($k_I R \approx 0.45F_\rho^{jt} R/u$) relative to a purely adiabatic jet. For example, the adiabatic Mach 1.5 transmagnetosonic jet shows an increase in the growth rate associated with the symmetric surface wave S1, whereas we find a decrease on the cooling jet. However, in general, the remaining solutions exhibit a typical adiabatic transmagnetosonic structure that includes a monotonically increasing growth rate above some low-frequency cutoff associated with the first symmetric body wave, a decrease in the maximum growth rate of the higher order body waves, a monotonically increasing growth rate associated with the asymmetric surface wave S, and a decrease in the maximum growth rate of all the asymmetric body waves (e.g., Hardee 1995).

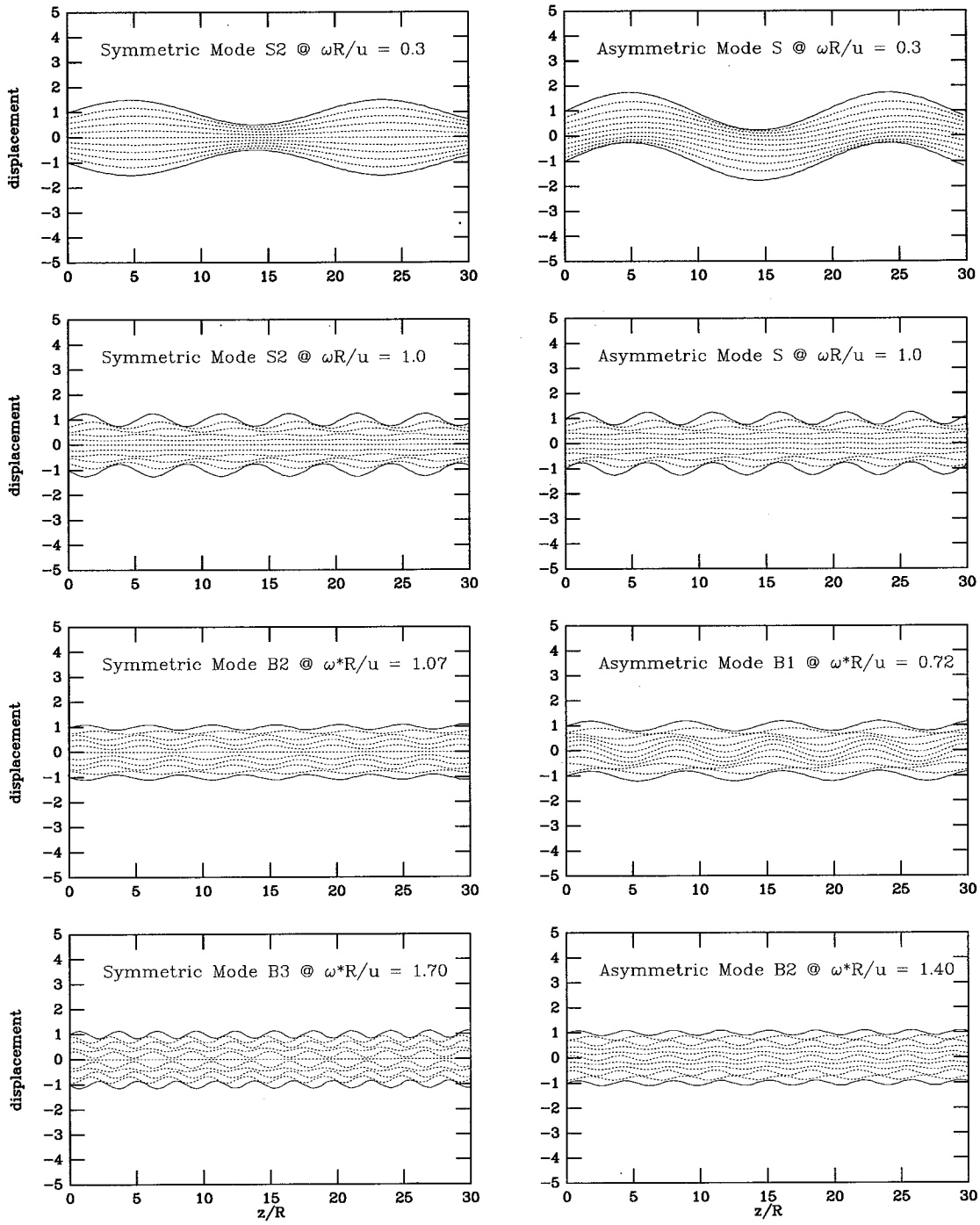

FIG. 5.—Fluid displacement surfaces produced by (1) the pinch mode surface wave (S2) at low and high frequencies, and body waves (B2, B3) at the fastest growing frequency, and (2) the sinusoidal mode surface wave (S) at low and high frequencies, and body waves (B1, B2) at the fastest growing frequency.

Some investigations of the effect of decreased jet thermal pressure to magnetic pressure were also performed for jet Mach numbers of 5.0, 3.0 and 1.5. In particular, a jet thermal pressure of only 10% of the total jet pressure showed an increase in the maximum growth rate of S1 by about a factor 4 relative to the growth rates shown in Figure 4, which were higher than the comparable adiabatic jet. However, in general, the solutions remained comparable to the results shown in Figure 4 for which the jet thermal pressure was 50% of the total pressure. This additional investigation suggested also that a decrease in the thermal pressure relative to the magnetic pressure, equivalent to decreasing the internal jet sound speed relative to the Alfvén speed, results in solutions to the dispersion relation that resemble more closely the adiabatic jet results for comparable parameters. Our present results indicate that cooling and adiabatic jets become more similar in their stability properties as the magnetic field becomes more important and is the expected result for $V_A^2 \gg a^2/Q$. Thus, the suppression of body waves associated with fast magnetosonic waves found on the adiabatic, internally submagnetosonic and/or sub-Alfvénic jet is likely to remain true for the cooling jet as well. It is also likely that the asymmetric mode surface wave is stabilized on the sub-Alfvénic cooling jet just as is the case on the sub-Alfvénic adiabatic jet. Finally, we note that the symmetric mode surface

wave and symmetric and asymmetric mode body waves associated with slow magnetosonic waves can become weakly unstable in some restricted parameter regimes on the sub-Alfvénic adiabatic jet, and that this should remain true for the cooling jet examined here.

5. TRANSVERSE STRUCTURE OF SYMMETRIC AND ASYMMETRIC MODES

The total pressure, radial velocity, and radial displacement perturbations inside the jet associated with the asymmetric sinusoidal modes of the slab jet are given by

$$p_1^*(x) = p_{1s}^* \frac{\sin(\beta_{jt} x)}{\sin(\beta_{jt} R)} \exp[i(k_z z - \omega t)],$$

$$u_{x1}(x) = u_{x1s} \frac{\cos(\beta_{jt} x)}{\cos(\beta_{jt} R)} \exp[i(k_z z - \omega t)], \tag{21}$$

$$\xi_x(x) = \xi_{xs} \frac{\cos(\beta_{jt} x)}{\cos(\beta_{jt} R)} \exp[i(k_z z - \omega t)],$$

where p_{1s}^*, u_{x1s}, and ξ_{xs} are the surface amplitudes of the total pressure, the radial velocity, and the radial displacement perturbations, respectively, and $\beta_{jt}(\omega, k)$ (ω and k are normal mode solutions of the asymmetric dispersion relation). Note that $D\xi_x/Dt = u_{x1}$ and therefore that $\xi_x(x) \propto u_{x1}(x)/(\omega - ku)$. In equations (21), $\sin(\beta_{jt} x)/\sin(\beta_{jt} R)$ is replaced by $\cos(\beta_{jt} x)/\cos(\beta_{jt} R)$, and $\cos(\beta_{jt} x)/\cos(\beta_{jt} R)$ is replaced by $\sin(\beta_{jt} x)/\sin(\beta_{jt} R)$ for the symmetric mode. In general, the $\beta_{jt}(\omega, k)$ are complex, and the transverse behavior of perturbations associated with the normal modes inside the jet can be written in the form $f(x) = A(x)e^{i\phi(x)} \exp[i(k_z z - \omega t)]$. There is both an amplitude and a phase dependence of the perturbation internal to the jet surface relative to the perturbation at the jet surface. In general, the amplitude dependence of the body waves leads to null surfaces between the jet center and the surface at which no fluid displacement occurs, one null surface for the first body wave, two null surfaces for the second body wave, etc., with fluid displacements in opposite directions on either side of the null surface.

Fluid displacements have been computed within the Mach 5 unmagnetized jet with DM-type cooling. Figure 5 shows the positions of displaced fluid surfaces associated with symmetric (S2) and asymmetric mode (S) surface waves at two frequencies, and with the symmetric mode second (B2) and third (B3) body waves and asymmetric mode first (B1) and second (B2) body waves at each wave's maximally growing frequency. We note that symmetric modes S1 and B1 both show the same structure as S2 at $\omega R/u = 0.3$, but with different wavelength. A more typical structure for the symmetric mode body wave B1, determined by computing the structure associated with B1 on the adiabatic jet, shows a phase shift in the displacement between jet surface and jet center of about one-quarter wavelength. Thus, the symmetric mode body wave B1 behaves like a surface wave and is strongly coupled to S1 and S2 on the jet with DM-type cooling, as is suggested by the structure of the solutions shown in Figure 2. While the behavior of the surface waves is unchanged at lower frequencies, there is a rapid change as frequencies rise: by frequency $\omega R/u = 1.0$, the jet can no longer respond as a unit to the surface oscillations. In general, at frequencies above $\omega R/a_{ex} \approx 2$ (for Mach 5, this becomes $\omega R/u \approx 0.4$, and for Mach 20, $\omega R/u \approx 0.1$), displacements decrease considerably in amplitude and are shifted in phase as the distance from the jet surface increases, a central jet core is only marginally displaced, and only internal waves are produced (cf. Hardee et al. 1994). Considerably more interior displacement is revealed to accompany the symmetric mode body wave B2 and the asymmetric mode body wave B1. Both of these modes reveal significant displacements of a jet core considerably out of phase with displacements outside a null displacement surface at about 75% of the jet radius. The symmetric mode body wave B3 and the asymmetric mode body wave B2 also reveal displacement of a jet core, but now interior to a null displacement surface at about 25% of the jet radius. A second null displacement surface is located at about 75% of the jet radius. With the exception of the symmetric mode S2 at $\omega R/u = 0.3$, surface amplitudes in Figure 5 have been chosen at the maximum amplitude for which displacement surfaces do not cross. At least approximately, this choice must represent the maximum possible amplitude since larger displacements imply the development of shocks where displacement surfaces cross. Note that the maximum surface amplitude decreases either as the frequency increases or for the higher order body waves. Such a result is consistent with the fact that motions in the transverse direction cannot greatly exceed the jet magnetosonic speed and that the displacement $\xi_x(x) \propto u_{x1}(x)/[\omega_m(1 - k_m u/\omega_m]$, where $u_{x1}(x) \leq a_{ms,jt}$. Thus, as ω_m increases for a surface wave or for the fastest growing higher order body waves at ω_m^*, the maximum displacement should decrease. We conclude that the largest displacements should be associated with the surface waves at frequencies $\omega R/a_{ex} < 2$ and/or associated with the lowest order body waves at higher frequencies.

6. SUMMARY

In this paper, we have presented a linear stability analysis for K-H modes in astrophysical jets in which radiative cooling is dynamically important. Both magnetized and unmagnetized jets were studied. Moreover, we have performed our analysis using two separate cooling curves, one due to Dalgarno & McCray (1972; the DM cooling curve), which is appropriate for interstellar gas, and the other due to MacDonald & Bailey (1981; the MB cooling curve), which is appropriate for photoionized gas. The DM cooling curve is applicable to studies of protostellar jets, while the MB curve is applicable to jets from active galactic nuclei. By studying two cooling curves, we have been able to investigate in detail the influence of cooling on the dynamical properties of K-H modes in jets.

We have found significant differences in the properties of the K-H modes in a jet between DM and MB cooling curves, and in comparison with the adiabatic jet. In particular, the MB cooling curve is such a steep function of temperature, proportional

to $T^{2.53}$, that linear perturbations away from the equilibrium state (where the cooling and heating rates are balanced) tend to be damped. However, the opposite is true for the DM cooling curve. In this case, at temperatures above and below 10,000 K, the cooling rate is a less steep function of temperature, proportional to $T^{0.5}$, so that the growth of linear perturbations tends to be enhanced by the increase in the heating rate compared with cooling in dense regions.

It is conventional to classify K-H modes on a jet into two families: surface waves and body waves. In general, DM cooling tends to increase the growth rate of the K-H *surface* waves relative to the adiabatic jet, whereas MB cooling tends to decrease their growth rate. The changes in the growth rate relative to the adiabatic case are stronger for the symmetric pinch surface wave than for the asymmetric sinusoidal surface wave. In fact, we find that the growth rate of the pinch surface wave can become comparable to that of the sinusoidal surface wave (instead of much less, as in the case of the adiabatic supermagnetosonic jet). We also note that the single pinch surface wave on the adiabatic jet splits into two pinch surface waves on the cooling jet, with a strong interaction evident between these surface waves and the first pinch body wave.

For our choice of parameters, a cold jet with $n_{jt} = 600$ cm^{-3}, $T_{jt} = 1000$ K, and a hot external cocoon medium with $n_{ex} = 60$ cm^{-3} $T_{jt} = 10{,}000$ K, DM cooling can enhance greatly the growth rate of the *surface* waves, particularly at low and high frequencies relative to the maximally growing frequency associated with the adiabatic jet, i.e., we find that there can be broad ranges of frequencies and wavelengths for which the growth rates are nearly constant. A growth rate plateau at low frequencies arises from internal jet cooling, and a growth rate plateau at high frequencies arises from external cocoon cooling. If the ionization fraction in the jet is higher than our choice of $n_e/n = 0.001$, the internal jet cooling rate is larger, and the low-frequency growth rate of the pinch surface wave is increased proportionally. There is a slight effect on the sinusoidal surface wave at low frequencies. On the other hand, the DM cooling time for our choice of cocoon temperatures and densities is on the order of 10 yr. This suggests that the cocoon surrounding a real protostellar jet will be cooler than 10,000 K, and a more realistic choice of cooling rate would place the external cocoon medium on the steep temperature discontinuity of the DM cooling curve. In this case, the high-frequency stability behavior would be more like our MB cooling results (cocoon cooling time of about 550 yr), which led to a maximum in the growth rate, albeit at a frequency and wavelength different from the adiabatic case, and wave damping at higher frequencies. We note that at the highest frequencies and correspondingly shortest perturbation wavelengths, adiabatic and cooling jets are predicted to behave similarly and with negligible growth rates.

The effect of cooling on pinch and sinusoidal *body* waves that accompany the surface wave can also be significant. In general, asymmetric body waves of all order and symmetric body waves of higher than first order are affected similarly by cooling. For DM cooling, the growth of body waves occurs over a reduced frequency range, and the maximum growth rate is somewhat reduced relative to the adiabatic jet. The maximum growth rate of body waves is less than the growth rate of the surface waves at the same frequency. For MB cooling, the maximum growth rate of the body waves remains comparable to the adiabatic jet, and the body waves grow more rapidly than the surface waves. The principal effect of MB cooling on the body waves is to greatly narrow the frequency range over which these waves are growing. There are small shifts in the maximally growing frequency of the body waves as a function of the cooling rate and cooling function.

Provided a jet is highly supermagnetosonic and not magnetic pressure–dominated, the introduction of a magnetic field changes some details of the structure of the solutions to the dispersion relations but does not strongly modify the important differences between an adiabatic jet and a DM cooling jet. For example, the high-frequency growth rate plateau associated with pinch and sinusoidal surface waves, and the frequencies and wavelengths associated with the maximum growth rate of the body waves, remain nearly unchanged from the purely fluid results. However, when the jet is magnetic pressure–dominated or when the jet is not highly supermagnetosonic, the stability properties become much more similar to those of the adiabatic jet. In the present analysis, the most important effect of a decrease in the magnetosonic Mach number or an increase in the magnetic pressure is to eliminate the high-frequency plateau in the growth rate associated with pinch and sinusoidal surface waves.

For the first time, we have also investigated the structures expected to arise as the result of growth associated with the various wave modes by plotting fluid displacement surfaces. With the exception of the two pinch surface and first pinch body waves, all displacement structures remain similar on adiabatic and cooling jets. The most important aspect of this investigation for cooling jets is the change in structure of the surface waves as a function of frequency. For example, at higher frequencies, the jet cannot respond bodily to either pinching or sinusoidal oscillation, the surface perturbation is not communicated strongly into the interior, and the maximum amplitude is reduced. The most important implication of this result is that high growth rates will not necessarily imply large jet distortion since the jet cannot respond bodily to the short wavelengths associated with the higher frequencies. In the present context, we have found that large-scale pinching or sinusoidal distortion should occur only for perturbation frequencies $\omega R/a_{ex} < 2$. Higher perturbation frequencies can produce only relatively small-amplitude short-wavelength ripples to the jet surface via the surface wave and/or relatively larger amplitude short-wavelength rippling internal structures via the body waves.

It is not possible to compare directly our results for the pinching mode with those of Massaglia et al. (1992) because they used a different cooling function, they performed a temporal analysis, rather than the spatial stability analysis performed here, and they only analyzed the effect of cooling on K-H growth at two wavenumbers on a cylindrical jet and not on the slab jet analyzed here. However, preliminary results indicate a similar cooling response in slab and cylindrical geometries as was previously found for the adiabatic jet by Hardee & Norman (1988). Very approximately, the short- and long-wavelength cases of $kR = 5$ and $kR = 0.5$ on the Mach number $M_{jt} = 10$ jet investigated by Massaglia et al. correspond to frequencies of $\omega R/u \approx 4$–5 and $\omega R/u \approx 0.4$–0.5, respectively, on our Mach number $M_{jt} = 15.8$ and 63.2 jets. We note that their long-wavelength case is not truly at long wavelength and low frequency but is closer to intermediate wavelength and frequency. Our ratio of cooling time to dynamical time, $\tau \equiv t_{cool}/t_{dyn}$, where $t_{dyn} \equiv R/a_{jt} = 6.7 \times 10^9$ s, is $\tau = 5.4$ for DM cooling, with $t_{cool}^{DM} \equiv (\Gamma - 1)^{-1} p_{jt}/\mathcal{C}_{jt}^{DM} = 3.6 \times 10^{10}$ s, and $\tau = 8.8$ for MB cooling, with $t_{cool}^{MB} \equiv (\Gamma - 1)^{-1} p_{jt}/\mathcal{C}_{jt}^{MB} = 5.9 \times 10^{10}$ s. These

values of τ are at the upper limits shown by Massaglia et al. While direct comparison is not possible, we do appear to agree with several of their conclusions: (1) the growth rate of body waves can be reduced by DM cooling, (2) the growth rate of pinching (axisymmetric) and sinusoidal (asymmetric) surface waves can be similar at high frequency and short wavelength but different at intermediate and longer wavelengths, and (3) these linear results are insensitive to the Mach number. On the other hand, relative growth rates appear to depend sensitively on the magnitude and temperature dependence of the cooling function, which is illustrated by the significantly different growth rates found for DM cooling and MB cooling.

In Paper II, we perform numerical simulations of slab jets with DM and MB cooling curves that verify the linear analysis results found here, extend the study of asymmetric instability into the nonlinear regime, examine the disruption of the jet into dense knots and filaments, and discuss the relevance of our results to observed protostellar jets.

P. E. H. acknowledges support from the National Science Foundation through grant AST 93-18397 to the University of Alabama, and J. M. S. acknowledges support by the NASA ATP through grant NAG-4202 to the University of Maryland.

REFERENCES

Begelman, M. C., & Cioffi, D. F. 1989, ApJ, 345, L21
Bertschinger, E. 1986, ApJ, 304, 154
Birkinshaw, M. 1991, in Beams and Jets in Astrophysics, ed. P. Hughes (Cambridge: Cambridge Univ. Press), 278
Blondin, J. M., Fryxell, B. A., & Königl, A. 1990, ApJ, 360, 370
Bührke, T., Mundt, R., & Ray, T. P. 1988, A&A, 200, 99 (BMR)
Chernin, L. W., Masson, C. R., Gouveia dal Pino, E. M., & Benz, W. 1994, ApJ, 426, 204
Cioffi, D. F., & Blondin, J. M. 1992, ApJ, 392, 458
Dalgarno, A., & McCray, R. A. 1972, ARA&A, 10, 375
Edwards, S., Ray, T. P., & Mundt, R. 1993, in Protostars and Planets III, ed. E. Levy & J. Lunine (Tucson: Univ. Arizona Press), 567
Eislöffel, J., Davis, C. J., Ray, T. P., & Mundt, R. 1994, ApJ, 422, L91
Falle, S. A. E. G., Innes, D. E., & Wilson, M. J. 1987, MNRAS, 225, 741
Gouviea dal Pino, E. M., & Benz, W. 1993, ApJ, 410, 686
———. 1994, ApJ, 435, 261
Hardee, P. E. 1995, in Ann. NY Acad. Sci., 773, Waves in Astrophysics, ed. J. Hunter & R. Wilson, 14
Hardee, P. E., & Clarke, D. A. 1995, ApJ, 449, 119
Hardee, P. E., Clarke, D. A., & Howell, D. A. 1995, ApJ, 441, 644
Hardee, P. E., Cooper, M. A., & Clarke, D. A. 1994, ApJ, 424, 126
Hardee, P. E., Cooper, M. A., Norman, M. L., & Stone, J. M. 1992, ApJ, 399, 478 (HCNS)
Hardee, P. E., & Norman, M. L. 1988, ApJ, 334, 70
Hartigan, P., Morse, J. A., Heathcote, S., & Cecil, G. 1993, ApJ, 414, L121
Heathcote, S., Morse, J., Hartigan, P., Reipurth, B., Schwartz, R. D., Bally, J., & Stone, J. M. 1996, preprint
Hunter, J. H., & Whitaker, R. W. 1989, ApJS, 71, 777
MacDonald, J., & Bailey, M. E. 1981, MNRAS, 197, 995
Massaglia, S., Trussoni, E., Bodo, G., Rossi, P., & Ferrari, A. 1992, A&A, 260, 243
Noriega-Crespo, A., Garnavich, P. M., Raga, A. C., Cantò, J., & Böhm, K.-H. 1996, ApJ, 462, 804
Norman, M. L., Winkler, K.-H., & Smarr, L. L. 1983, in Astrophysical Jets, ed. A. Ferrari & A. G. Pachoczyk (Dordrecht: Reidel), 227
Ray, T. P. 1996, in Proc. NATO ASI, Solar and Astrophysical MHD Flows, ed. K. Tsinganos (Dordrecht: Kluwer), in press
Ray, T. P., Mundt, R., Dyson, J. E., & Falle, S. A. E. G. 1996, ApJ, 468, L103
Raymond, J. C., Cox, D. P., & Smith, B. W. 1976, ApJ, 204, 290
Reipurth, B. 1989, Nature, 340, 42
Reipurth, B., & Cernicharo, J. 1995, in Rev. Mexicana Astron. Astrofis. Ser. Conf. 1, Circumstellar Disks, Outflows and Star Formation, ed. S. Lizano & J. M. Torrelles (México, D.F.: Inst. Astron, UNAM), 43
Shapiro, P. R., & Moore, R. T. 1976, ApJ, 207, 460
Spitzer, L. 1978, Physical Processes in the Interstellar Medium (New York: Wiley)
Stone, J. M., & Norman, M. L. 1993a, ApJ, 413, 198
———. 1993b, ApJ, 413, 210
———. 1994, ApJ, 420, 237
Stone, J. M., Xu, J., & Hardee, P. E. 1997, ApJ, in press (Paper II)